Microwave Magnetics

Micromagnetic Modeling of Parametric Amplification of Forward Volume Spin Waves by Noncollinear Surface Acoustic Waves

Carson Rivard, Albrecht Jander, and Pallavi Dhagat

School of Electrical Engineering and Computer Science, Oregon State University, Corvallis, OR 97331, USA

Received 13 Aug 2024, revised 24 Sep 2024, accepted 7 Oct 2024, published 14 Oct 2024, current version 26 Nov 2024.

Abstract—Micromagnetic modeling is used to simulate the parametric amplification of forward volume spin waves by a surface acoustic wave (SAW) traveling noncollinearly in a yttrium–iron–garnet thin film. The angle of incidence between the signal spin wave and the SAW pump determines the strength of parametric coupling as well as the propagation direction of the resulting idler spin wave. In a collinear arrangement, where the spin wave and SAW travel together, the acoustic pump amplitude needed to achieve amplification is greater than the threshold for the parametric generation of spin waves from the thermal background. However, in a noncollinear arrangement with $>35°$ angle of incidence between the signal spin wave and SAW pump, the coupling is enhanced and allows for continuous amplification of spin waves by more than $10\times$ without simultaneously resulting in unconstrained growth of thermal spin waves. The angular dependence of the parametric coupling strength, as determined from the simulations, agrees qualitatively with theoretical predictions.

Index Terms—Microwave magnetics, micromagnetic modeling, parametric interactions, spin waves, surface acoustic waves.

I. INTRODUCTION

Spin waves are promising as information carriers for analog radio frequency (**RF**) signal processing [Adam 1988, Chumak 2017, Wang 2018, Hansen 2020], but the space and time over which they can propagate, and thus the complexity of functions that can be implemented, are limited by damping. Parametric pumping, a form of nonlinear three-wave mixing in which a "pump" wave parametrically amplifies a "signal" wave and, in the process, produces a third "idler" wave, can be used to compensate for spin wave decay. Parametric pumping by an RF magnetic field, oriented parallel to the static magnetization, has been most thoroughly studied (see Brächer [2017] for a review). However, since it requires Ørsted fields from current-carrying wires, this so-called "parallel pumping" technique suffers from poor efficiency due to Joule heating. Further, parallel pumping is possible only on elliptical spin precession, making it ineffective for amplifying forward-volume spin wave modes that are attractive for device applications due to their isotropic propagation characteristics and single-valued dispersion relation. More recently, spin wave amplification employing voltage-controlled magnetic anisotropy (**VCMA**) [Verba 2017, Deka 2022] and spin-orbit torque (**SOT**) [Divinskiy 2018] has been demonstrated.

The amplification mechanism studied here—by micromagnetic simulation—is the parametric pumping of spin waves by surface acoustic waves (**SAW**s), which offer three benefits. First, SAWs are practical for application, having already long been implemented in miniaturized low-power RF signal processing devices at commercial scale [Yang 2022]. Second, the coupling of acoustic waves to spin waves is mediated via magnetostrictive modulation of anisotropy rather than Ørsted fields, promising efficiency similar to VCMA and SOT devices. Third, unlike amplification with VCMA and SOT, using a wave for the pump provides an additional degree of freedom to separate the amplified wave and idler signals by direction of propagation in addition to frequency and phase.

The principle of acoustic parametric pumping of spin waves is well established [Matthews 1967, Lisenkov 2019] and has been demonstrated with bulk acoustic wave pumps in yttrium–iron–garnet (**YIG**) rods [Matthews 1964] and films [Chowdhury 2017]. Recently, SAW pumping of spin waves from a thermal background was reported [Geilen 2024]. The amplification of coherent spin waves (in the backward-volume wave geometry) by SAW pumping has also been shown in micromagnetic simulation [Mohseni 2023] but has not yet been experimentally investigated.

The simulations presented here further these studies by investigating parametric pumping of forward-volume spin waves by SAWs in an out-of-plane biased YIG film. YIG is chosen because it has low spin wave damping and moderate magnetoelastic coupling. In addition, depending on the crystal cut of YIG, both types of waves display nearly isotropic propagation in the film plane, allowing for the angle of incidence between the spin wave and the acoustic pump wave to be changed arbitrarily. As we show here, the noncollinear arrangement can enhance the parametric coupling strength to allow amplification of a coherent spin wave without the unconstrained pumping of thermal spin waves.

II. THEORY

A. Conservation Laws

In the parametric interaction, the conservation of energy and momentum constrains the frequencies, ω, and wave vectors, $\boldsymbol{k}$, of the three waves

$$\omega_p = \omega_s + \omega_i \tag{1}$$

$$\boldsymbol{k}_p = \boldsymbol{k}_s + \boldsymbol{k}_i \tag{2}$$

where the subscripts p, s, and i denote pump, signal, and idler, respectively.

Corresponding author: Albrecht Jander (e-mail: jander@oregonstate.edu).
Digital Object Identifier 10.1109/LMAG.2024.3479922

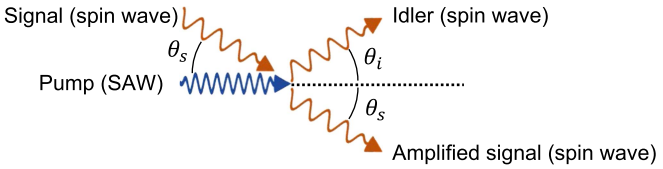

Fig. 1. Illustration of the parametric interaction between a spin wave and a noncollinear SAW pump.

In the case of conventional parallel pumping, the microwave pump *photon* has negligible momentum in comparison to the magnons. The signal and idler magnons resulting from the interaction, therefore, have nearly equal and opposite wavevectors ($\boldsymbol{k}_i = -\boldsymbol{k}_s$) and, if the dispersion is isotropic, also equal frequency ($\omega_i = \omega_s = \omega_p/2$). For acoustic pumping, on the other hand, the pump *phonons* carry momentum of magnitude similar to that of the magnons, and the vector nature of relation (2) becomes relevant. If the acoustic pump propagates at an angle θ_s relative to the signal spin wave, as in Fig. 1, the idler travels away at a different angle θ_i with momentum conservation requiring

$$\left|\boldsymbol{k}_p\right| = \left|\boldsymbol{k}_s\right| \cos(\theta_s) + |\boldsymbol{k}_i| \cos(\theta_i) \tag{3}$$

$$0 = |\boldsymbol{k}_s| \sin(\theta_s) + |\boldsymbol{k}_i| \sin(\theta_i). \tag{4}$$

For the degenerate case (i.e., the condition $\omega_s = \omega_p/2$) studied here, ω_s will equal ω_i by (1). Since the dispersion is isotropic in the plane, $|\boldsymbol{k}_s|$ will equal $|\boldsymbol{k}_i|$, and, from (3) and (4), it follows that the signal and idler will propagate away from the pump with equal wavenumber, but opposite angles

$$|\boldsymbol{k}_s| = |\boldsymbol{k}_i| = |\boldsymbol{k}_p|/2\cos(\theta_s) \tag{5}$$

$$\theta_i = -\theta_s. \tag{6}$$

(If the pump is not at exactly twice the signal frequency, the idler wave may be shifted both in frequency and angle.) Although (5) and (6) are valid for $0^\circ < \theta_s < 90^\circ$, the simulations presented here examine only angles in the range $0^\circ < \theta_s < 50^\circ$, as approaching $\theta_s = 90^\circ$ demands increasingly shorter spin wave wavelengths to satisfy (5) and, consequently, computationally intractable finer discretization in the micromagnetic model.

B. Acoustic and Spin Wave Equations

In this section, the equations for the SAW and spin waves are described, and then we derive an expression for the strength of parametric coupling. The acoustic wave, assumed to be travelling in the x direction, is given by

$$\boldsymbol{u}(x,t) = \tilde{\boldsymbol{u}}\, e^{ik_p x} e^{-i\omega_p t} \tag{7}$$

where $\tilde{\boldsymbol{u}}$ is a matrix representing the amplitudes of the strain components of the wave.

SAWs are a combination of shear and tensile strain waves. Most generally, the strain components of the wave can be expressed by the matrix

$$\tilde{\boldsymbol{u}} = \begin{bmatrix} \tilde{u}_{xx} & \tilde{u}_{xy} & \tilde{u}_{xz} \\ \tilde{u}_{yx} & \tilde{u}_{yy} & \tilde{u}_{yz} \\ \tilde{u}_{zx} & \tilde{u}_{zy} & \tilde{u}_{zz} \end{bmatrix} \tag{8}$$

in which u_{ii} are tensile strains and $u_{ij} (i \neq j)$ are shear strains.

In crystalline substrates, the strain components of a SAW depend on the orientation of the crystal axes with respect to the surface as well as the direction of SAW propagation. In this work, surface strain component amplitudes calculated for SAWs traveling in a ⟨111⟩ direction on a ⟨111⟩ cut crystalline YIG substrate [Slobodnik 2005] are used such that

$$\tilde{\boldsymbol{u}} = u_0 \begin{bmatrix} 1 & i\,7.14\cdot 10^{-2} & i\,1.74\cdot 10^{-3} \\ i\,7.14\cdot 10^{-2} & 0 & i\,1.22\cdot 10^{-2} \\ i\,1.74\cdot 10^{-3} & i\,1.22\cdot 10^{-2} & -0.4202 \end{bmatrix}. \tag{9}$$

The negative sign on $\tilde{u}_{zz}$ indicates that the normal strain is 180° out of phase with the longitudinal strain, $\tilde{u}_{xx}$. The i in the off-diagonal components indicates that the shear strain components of the SAW are 90° out of phase with the tensile strain components. In the remainder of this letter, the amplitude, u_0, of the longitudinal strain component is used to represent the SAW strain amplitude.

The two spin waves (signal and idler) are described by

$$\boldsymbol{s}_v = \tilde{\boldsymbol{s}}_s\, e^{i\boldsymbol{k}_s\cdot\boldsymbol{r}} \quad \boldsymbol{s}_{v'} = \tilde{\boldsymbol{s}}_i\, e^{i\boldsymbol{k}_i\cdot\boldsymbol{r}}. \tag{10}$$

For the forward-volume spin waves, the polarization vectors

$$\tilde{\boldsymbol{s}}_s = \begin{bmatrix} \cos\theta_s - i\epsilon\,\sin\theta_s \\ \sin\theta_s + i\epsilon\,\cos\theta_s \\ 0 \end{bmatrix} \quad \tilde{\boldsymbol{s}}_i = \begin{bmatrix} \cos\theta_s + i\epsilon\,\sin\theta_s \\ -\sin\theta_s + i\epsilon\,\cos\theta_s \\ 0 \end{bmatrix} \tag{11}$$

describe the precession of the spins about the z-axis with ellipticity ϵ for waves travelling at angles θ_s and $\theta_i = -\theta_s$, respectively (with $\epsilon = 1$ being circular precession).

C. Strength of Parametric Interaction

Lisenkov [2019] derived a theoretical framework for calculating the parametric coupling between an acoustic wave and spin waves. Their central result in this framework

$$V_{vv'} = -i\frac{\gamma}{\mathcal{A}_v}\int \left[\boldsymbol{s}^\dagger_{v'}(\boldsymbol{r})\cdot\boldsymbol{s}^\dagger_v(\boldsymbol{r})\right]\left[\boldsymbol{\mu}(\boldsymbol{r})\cdot\hat{\boldsymbol{T}}(\boldsymbol{r})\cdot\boldsymbol{\mu}(\boldsymbol{r})\right] d^3\boldsymbol{r} + i\frac{\gamma}{\mathcal{A}_v}\int \left[\boldsymbol{s}^\dagger_{v'}(\boldsymbol{r})\cdot\hat{\boldsymbol{T}}(\boldsymbol{r})\cdot\boldsymbol{s}^\dagger_v(\boldsymbol{r})\right] d^3\boldsymbol{r} \tag{12}$$

is a general expression for the coupling strength between an acoustic wave and the two spin waves.

Parametric pumping of spin waves by acoustic waves occurs via inverse magnetostriction, by which a time-varying strain modulates the magnetic anisotropy. In (12), the effective anisotropy produced by the acoustic wave is expressed via the tensor operator

$$\hat{\boldsymbol{T}}_{kl} = 2b_{ijkl}u_{ij}/M_s \tag{13}$$

where b_{ijkl} are the components of the magnetoelastic tensor, M_s is the saturation magnetization, and u_{ij} are the strain components of the acoustic wave in (7). For a crystal with cubic symmetry, such as YIG, only $b_{iiii} = B_1$ and $b_{ijij} = B_2$ $(i \neq j)$ are nonzero, yielding

$$\hat{\boldsymbol{T}} = \frac{2}{M_s}\begin{bmatrix} B_1\tilde{u}_{xx} & B_2\tilde{u}_{xy} & B_2\tilde{u}_{xz} \\ B_2\tilde{u}_{yx} & B_1\tilde{u}_{yy} & B_2\tilde{u}_{yz} \\ B_2\tilde{u}_{zx} & B_2\tilde{u}_{zy} & B_1\tilde{u}_{zz} \end{bmatrix} e^{ik_p x} \tag{14}$$

where the time dependence, $e^{-i\omega_p t}$, is not included.

In (12), γ is the gyromagnetic constant, $\mathcal{A}_v$ is the mode norm, and $\boldsymbol{\mu}(\boldsymbol{r})$ is a unit vector in the direction of equilibrium magnetization.

For forward-volume waves, this is uniform in $\boldsymbol{r}$ and oriented in the z direction

$$\boldsymbol{\mu} = \begin{bmatrix} 0 \\ 0 \\ 1 \end{bmatrix}. \tag{15}$$

Evaluating (12) using wave equations (7) through (11) and definitions (13) through (15) leads to the following result for noncollinear pumping of forward volume waves:

$$V_{vv'}(\theta_s) = i\gamma \frac{2B_1}{M_s} \frac{\tilde{u}_{xx}(\cos\theta_s + i\epsilon\sin\theta_s)^2 - i\tilde{u}_{zz}\left(1-\epsilon^2\right)\cos 2\theta_s}{2\epsilon} \tag{16}$$

Considering the numerator, the right-hand term is the effect of the strain component, $\tilde{u}_{zz}$, parallel to the equilibrium magnetization. As in parallel pumping with an RF field, this term is operative only when the time-varying component of magnetization along the strain axis oscillates due to elliptical spin precession (i.e., when $\epsilon > 1$). The ellipticity in forward-volume spin waves becomes significant only when the wavelength is short compared to the film thickness. The ellipticity can be calculated from $\epsilon = \omega_s / \gamma B_{\text{eff}}$ [Stancil 2009] for effective *internal* bias field, B_{eff}, which includes the demagnetizing and anisotropy fields.

The left-hand term is the effect of the longitudinal strain component, $\tilde{u}_{xx}$, perpendicular to the magnetization. However, the action of $\tilde{u}_{xx}$ is fundamentally different from a perpendicular RF field because the induced time-varying anisotropy has an *axis* rather than a *direction*. As a result, the magnetization precession is forced *twice* in an acoustic period, and the parametric pumping of even circularly precessing moments (i.e., with $\epsilon = 1$) becomes possible.

In (16), at some angles of incidence, the effects of the $\tilde{u}_{xx}$ and $\tilde{u}_{zz}$ strain components can work together to enhance the pumping, while at other angles the phasing is such that their contributions counteract. This leads to the angular dependence of the parametric coupling strength.

Finally, the threshold SAW strain amplitude, u_{th}, at which the parametric coupling overcomes the spin wave damping and amplification can occur is

$$u_{\text{th}} = \Gamma / |V_{vv'}(\theta_s)| \tag{17}$$

where $\Gamma = \alpha\omega_s$ is the spin wave damping rate at frequency ω_s in a material with damping parameter α.

III. SIMULATION

Micromagnetic simulations of the interaction at 0 and 293 K are performed in MuMax3 [Vansteenkiste, 2014], with a conceptual device illustrated in Fig. 2. The YIG film, shown in gray, is assumed to be on a substrate with closely matched acoustic properties. (Gadolinium gallium garnet (**GGG**), the most commonly used substrate for YIG films, meets this requirement.) Transducers for SAWs and spin waves are atop the YIG film. In the simulation, however, the transducers are not explicitly modeled. Instead, the SAW is simulated as a spatially and temporally varying strain of 20 μm width and 4 GHz frequency (0.9 μm wavelength) with tensile components $\tilde{u}_{xx}$ and $\tilde{u}_{zz}$ and shear components $\tilde{u}_{xz}$, $\tilde{u}_{yz}$, and $\tilde{u}_{xy}$ as described in (9). These strain components, calculated at the YIG surface, are assumed to apply uniformly through the thickness of the film. The SAW strain amplitude, u_0, is varied from 30 ppm to 600 ppm. The spin wave transducer is modeled as a sinusoidal magnetic

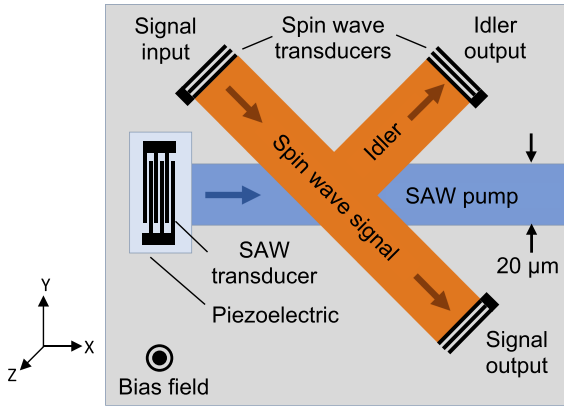

Fig. 2. Top view of the conceptual device structure for studying SAW pumping of spin waves.

field at 2 GHz. For any given SAW strain amplitude, the angle of incidence of the spin wave θ_s is varied from 0° to 50°. The out-of-plane bias field is tuned between 199 and 203 mT so that spin waves satisfying the wavelength condition in (5) are obtained at each angle. The spin wave beamwidth is 20 μm. The YIG film is 200 μm × 200 μm × 1 μm, discretized into 8192 cells × 8192 cells in a single layer. The material properties used for YIG are as follows: saturation magnetization, M_s = 140 kA/m; damping constant, $\alpha = 10^{-4}$ [Dubs 2017]; exchange stiffness, A = 2 pJ/m; cubic anisotropy constants $K_1 = -610$ J/m^3 and $K_2 = -26$ J/m^3 [Stancil 2009]; and magnetoelastic coupling coefficients $B_1 = 0.35$ MJ/m^3 and $B_2 = 0.7$ MJ/m^3 [Smith 1963]. To avoid reflection of spin waves from the edges of the simulated region, the damping is gradually increased to a value of 1 through the 512 cells at the border.

In MuMax3, the strain-dependent anisotropy is modeled as an effective magnetoelastic field, $\boldsymbol{B}_{\text{ME}}$. The given strain and current magnetization vector, $\boldsymbol{m}$, in each cell are used to obtain $\boldsymbol{B}_{\text{ME}}$ at every time step as

$$\boldsymbol{B}_{\text{ME}} = -\hat{\boldsymbol{T}} \cdot \boldsymbol{m}$$

$$\boldsymbol{B}_{\text{ME}} = -\frac{2}{M_s} \begin{bmatrix} B_1 m_x u_{xx} + B_2(m_y u_{xy} + m_z u_{xz}) \\ B_1 m_y u_{yy} + B_2(m_x u_{xy} + m_z u_{yz}) \\ B_1 m_z u_{zz} + B_2(m_y u_{yz} + m_x u_{xz}) \end{bmatrix}. \tag{18}$$

The back effect of the spin wave on the acoustic wave is not included.

The amplitudes of the signal input and output and idler spin waves are determined from the in-plane magnetization oscillations at 2 GHz, within a 0.01 GHz bandwidth and averaged across the beamwidths marked by the orange lines in Fig. 3. In each simulation, the input spin wave amplitude is fixed. Gain is defined as the signal or idler output amplitude divided by the input signal amplitude, and the signal-to-noise ratio (**SNR**) is calculated as the ratio of the 2 GHz component in the output signal to the rms value of all other spectral components.

IV. RESULTS AND DISCUSSION

Simulations without thermal fluctuations (i.e., at $T = 0$ K) show that a SAW can parametrically couple to a spin wave in both the collinear and noncollinear arrangements. The resulting steady-state spin wave beams after a simulation time of 1 μs are shown in Fig. 3 for select

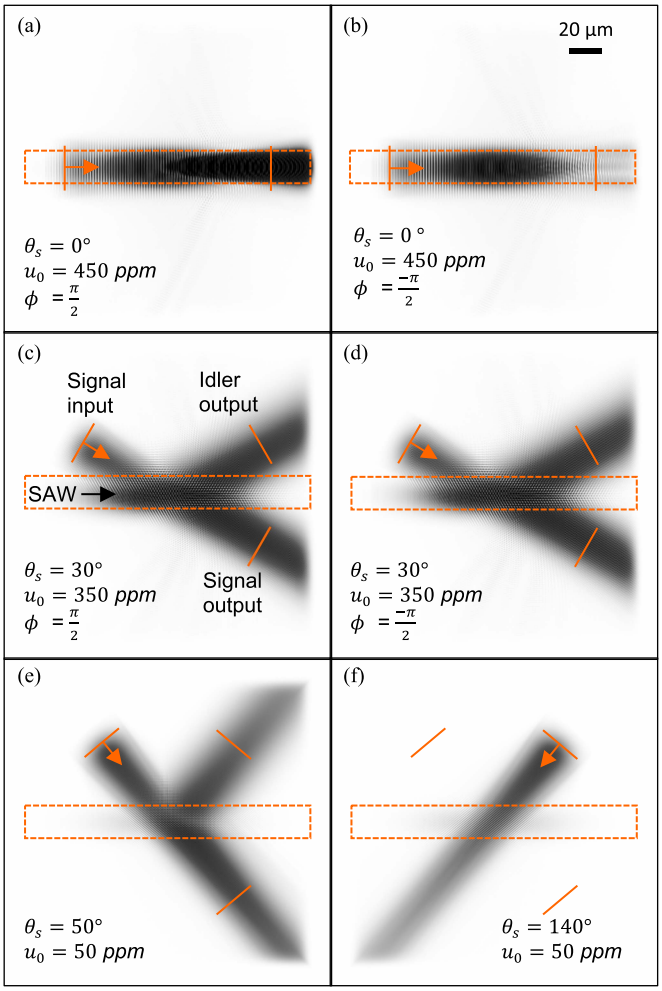

Fig. 3. Results at 0 K after 1 μs simulation time. The grayscale indicates the normalized in-plane magnetization component, m_x, of the spin waves. (a) and (b) Collinear arrangement with SAW phase, ϕ, of $\pi/2$ and $-\pi/2$. (c) and (d) Noncollinear arrangement with incident angle, $\theta_s = 30°$, and SAW phase of $\pi/2$ and $-\pi/2$. (e) $\theta_s = 50°$. (f) $\theta_s = 140°$. The dashed rectangle indicates the region in which the SAW strain is modeled. The simulated locations of input and output transducers are indicated by the orange lines, with arrows indicating the direction of spin wave propagation from the input transducer.

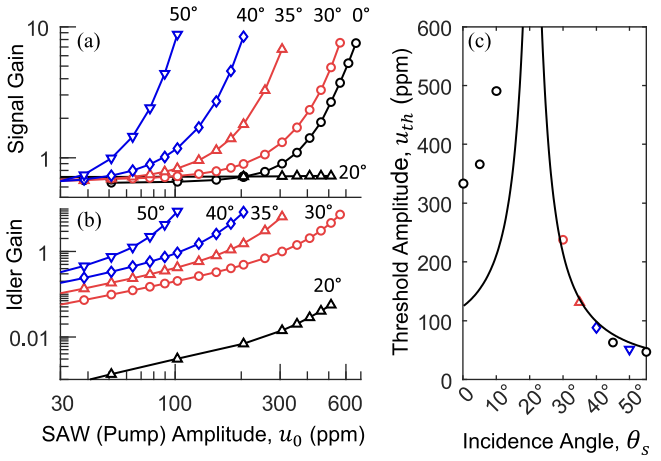

Fig. 4. Simulation results at 0 K. (a) Spin wave signal gain. (b) Idler gain as a function of SAW strain amplitude for varying angles of incidence. The results are plotted as symbols with lines as guide to the eye. (c) SAW strain needed to achieve unity signal gain versus angle of incidence. The simulation results (symbols) agree qualitatively with the theoretical prediction of (16) (curves).

cases of $\theta_s = 0°$ (collinear), 30°, 50°, and 140°. Coherent spin waves are generated at the signal input and propagate toward the "output" after traversing the SAW pumping region within the dashed rectangle. The parametric generation of the idler spin wave at the expected angle is clearly seen in Fig. 3(c)–(e). In the collinear arrangement in Fig. 3(a) and (b), the idler wave cannot be distinguished from the signal wave. However, amplification of the spin wave is clearly seen in Fig. 3(a). In the collinear case, the phase velocity of the SAW is equal to that of the spin wave, so the relative phase, ϕ, of the two waves remains constant throughout the interaction. This makes the gain sensitive to the SAW phase, resulting in amplification when the phase is $\frac{\pi}{2}$ [see Fig. 3(a)] and attenuation when the phase is $-\frac{\pi}{2}$ [see Fig. 3(b)]. In the noncollinear case, the phase velocities are unequal, and thus, the gain is independent of the SAW phase [see Fig. 3(c) and (d)]. Due to the propagation of SAW from left to right, the interaction results in a nonreciprocal device: spin wave excited at the input transducer can be transmitted to the idler output transducer [see Fig. 3(e)] but not if the two are interchanged [see Fig. 3(f)].

Fig. 4 shows the signal gain and idler gain as a function of incidence angle, θ_s, and SAW strain (pump) amplitude, u_0. A signal gain of greater than unity can be achieved given sufficient pump amplitude except for $\theta_s = 20°$.

The threshold pump amplitude, u_{th}, taken to be the SAW strain amplitude needed for a signal gain of 1, is plotted as a function of incidence angle in Fig. 4(c). The results agree qualitatively with the theoretical prediction in (16) using $\tilde{u}_{zz} = -0.42$ from (9). The discrepancy at lower angles is likely due to the finite beam widths used in the simulation, an effect that is not included in (16). At incidence angles in the vicinity of $\theta_s = 20°$, the coupling strength is reduced due to the counteraction of the perpendicular and in-plane components of the strain. Consequently, the threshold amplitude increases. The angle of minimum coupling, as seen from (16), depends on the particular elastic properties of the material and the ellipticity of the chosen wavelength.

For practical amplification of spin waves, it is important that spin wave modes present due to thermal fluctuations are not pumped more strongly than the signal spin wave, leading to unconstrained growth of spin waves pumped from the thermal background. Fig. 5 shows the time evolution of the signal and idler spin wave amplitudes at 293 K for various pump amplitudes. For pump amplitudes below 150 ppm, coherent spin waves with up to 10× amplification can be sustained. At higher pump amplitudes, the signal is overcome by spin waves pumped from the thermal background, and the SNR decreases abruptly. It should be noted that, due to the finite discretization, this simulation cannot model short-wavelength, higher order thickness modes that could also be pumped by the acoustic wave and prevent sustained amplification of the signal wave. Experimental verification of the modeled interactions will be necessary. The limitations of discretization notwithstanding, the simulations yield important insight into the angular dependence of the parametric coupling and thereby the design of practical SAW-pumped magnonic devices.

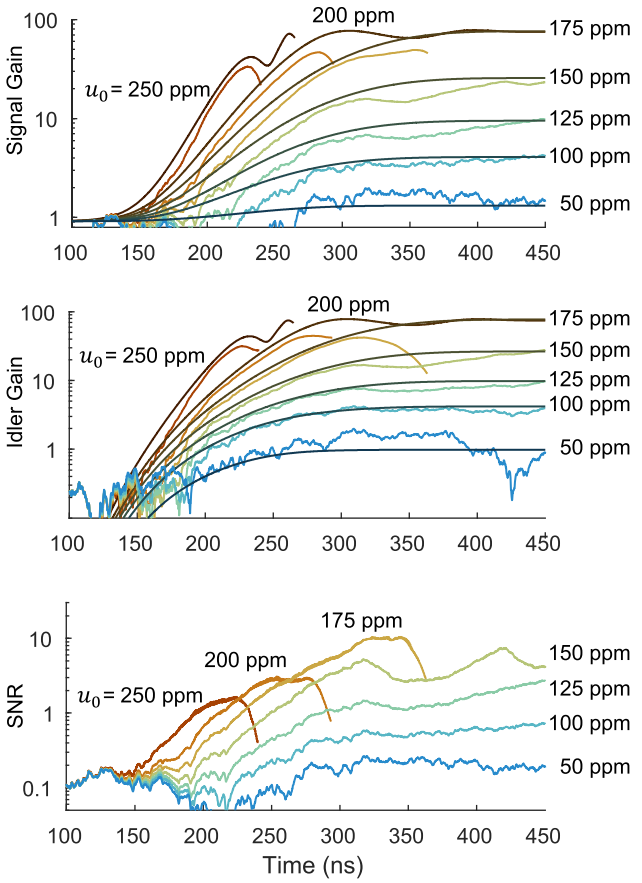

Fig. 5. Time evolution at 293 K of signal gain, idler gain, and SNR for $\theta_s = 45°$. For comparison, the results at 0 K are shown in thin (black) lines.

V. CONCLUSION

Noncollinear parametric pumping of forward-volume spin waves by SAWs is a promising way to achieve gain, nonreciprocity, and directional control in magnonic systems. With a high angle of incidence between the spin wave and acoustic pump, the parametric coupling strength is significantly enhanced compared with the collinear case, allowing for sustained amplification of signal spin waves with gains greater than 10 even in the presence of a thermal spin wave background. By compensating the damping losses that currently limit spin wave propagation length and time, SAW pumping can enable a new class of analog RF signal processing devices.

REFERENCES

Adam J D (1988), "Analog signal processing with microwave magnetics," *Proc. IEEE*, vol. 76, pp. 159–170, doi: 10.1109/5.4392.

Brächer T, Pirro P, Hillebrands B (2017), "Parallel pumping for magnon spintronics: Amplification and manipulation of magnon spin currents on the micron-scale," *Phys. Rep.-Rev. Sec. Phys. Lett.*, vol. 699, pp. 1–34, doi: 10.1016/j.physrep.2017.07.003.

Chowdhury P, Jander A, Dhagat P (2017), "Nondegenerate parametric pumping of spin waves by acoustic waves," *IEEE Magn. Lett.*, vol. 8, 3108204, doi: 10.1109/LMAG.2017.2737962.

Chumak A V, Serga A A, Hillebrands B (2017), "Magnonic crystals for data processing," *J. Phys. D: Appl. Phys.*, vol. 50, 244001, doi: 10.1088/1361-6463/aa6a65.

Deka A, Rana B, Anami R, Miura K, Takahashi H, Otani Y, Fukuma Y (2022), "Electric field induced parametric excitation of exchange magnons in a CoFeB/MgO junction," *Phys. Rev. Res.*, vol. 4, 023139, doi: 10.1103/PhysRevResearch.4.023139.

Divinskiy B, Demidov VE, Urazhdin S, Freeman R, Rinkevich A B, Demokritov S O (2018), "Excitation and amplification of spin waves by spin–orbit torque," *Adv. Mater.*, vol. 30, 1802837, doi: 10.1002/adma.201802837.

Dubs C, Surzhenko O, Linke R, Danilewsky A, Brückner U, Dellith J (2017), "Sub-micrometer yttrium iron garnet LPE films with low ferromagnetic resonance losses," *J. Phys. D: Appl. Phys.*, vol. 50, 204005, doi: 10.1088/1361-6463/aa6b1c.

Geilen M, Verba R, Nicoloiu A, Narducci D, Dinescu A, Ender M, Mohseni M, Ciubotaru F, Weiler M, Müller A, Hillebrands B, Adelmann C, Pirro P (2024), "Parametric excitation and instabilities of spin waves driven by surface acoustic waves," Adv. Phys. Res., doi: 10.1002/apxr.202400086.

Hansen M, Lisenkov I, Liu H, Jander A, Dhagat P (2020), "Correlation of binary-code-modulated microwave signals by parametric pumping of spin waves," *IEEE Magn. Lett.*, vol. 11, 5505105, doi: 10.1109/LMAG.2020.3017008.

Kittel C (1958), "Interaction of spin waves and ultrasonic waves in ferromagnetic crystals," *Phys. Rev.*, vol. 110, pp. 836–841, doi: 10.1103/PhysRev.110.836.

Lisenkov I, Jander A, Dhagat P (2019), "Magnetoelastic parametric instabilities of localized spin waves induced by traveling elastic waves," *Phys. Rev. B*, vol. 99, 184433, doi: 10.1103/PhysRevB.99.184433.

Matthews H, Lyons D H (1967), "Development program on magnetoelastic wave amplifier," Defense Technical Information Center, Sudbury, MA, USA, Tech. Rep. SRRC-CR-67-51.

Matthews H, Morgenthaler F R (1964), "Phonon-pumped spin-wave instabilities," *Phys. Rev. Lett.*, vol. 13, pp. 614–616, doi: 10.1103/PhysRevLett.13.614.

Mohseni M, Hamadeh A A, Geilen M, Pirro P (2023), "Amplification and frequency conversion of spin waves using acoustic waves," *IEEE Trans. Nanotechnol.*, vol. 22, pp. 806–810, doi: 10.1109/TNANO.2023.3331586.

Puebla J, Xu M, Rana B, Yamamoto K, Maekawa S, Otani Y (2020), "Acoustic ferromagnetic resonance and spin pumping induced by surface acoustic waves," *J. Phys. D: Appl. Phys.*, vol. 53, 264002, doi: 10.1088/1361-6463/ab7efe.

Rayleigh L (1885), "On waves propagated along the plane surface of an elastic solid," *Proc. London Math. Soc.*, vol. s1-17, pp. 4–11, doi: 10.1112/plms/s1-17.1.4.

Slobodnik A J, Conway E D, Delmonico R T (2005), "Microwave acoustics handbook, Vol. 1A, surface wave velocities," *J. Acoust. Soc. Amer.*, vol. 56, pp. 1307–1308, doi: 10.1121/1.1903432.

Smith A B, Jones R V (1963), "Magnetostriction constants from ferromagnetic resonance," *J. Appl. Phys.*, vol. 34, pp. 1283–1284, doi: 10.1063/1.1729473.

Stancil D, Prabhakar A (2009), *Spin Waves: Theory and Applications*. Berlin, Germany: Springer, doi: 10.1007/978-0-387-77865-5.

Vansteenkiste A, Leliaert J, Dvornik M, Helsen M, Garcia-Sanchez F, Van Waeyenberge B (2014), "The design and verification of MuMax3," *AIP Adv.*, vol. 4, 107133, doi: 10.1063/1.4899186.

Verba R, Carpentieri M, Finocchio G, Tiberkevich V, Slavin A (2017), "Excitation of spin waves in an in-plane-magnetized ferromagnetic nanowire using voltage-controlled magnetic anisotropy," *Phys. Rev. Appl.*, vol. 7, 064023, doi: 10.1103/PhysRevApplied.7.064023.

Wang Q, Pirro P, Verba R, Slavin A, Hillebrands B, Chumak A V (2018), "Reconfigurable nanoscale spin-wave directional coupler," *Sci. Adv.*, vol. 4, e1701517, doi: 10.1126/sciadv.1701517.

Yang Y, Dejous C, Hallil H (2022), "Trends and applications of surface and bulk acoustic wave devices: A review," *Micromachines (Basel)*, vol. 14, 43, doi: 10.3390/mi14010043.